Nanostructuring Titania: Control over Nanocrystal Structure, Size, Shape, and Organization

Abdelkrim Chemseddine*[a] and Thomas Moritz[b]

Dedicated to Professor J. Rouxel in recognition of his important contributions to the chemistry of solids

Keywords: TiO_2 / Growth / Self-organisation / Polytitanate / Nanocrystals / Nanostructure / Superlattice / Films

Control over crystal structure, size, shape, and organization of TiO_2 nanocrystals has been achieved by means of wet chemistry. Hydrolysis and polycondensation of titanium alkoxide [$Ti(OR)_4$] has been performed in the presence of tetramethylammonium hydroxide (Me_4NOH). This base both catalyzes the reaction and provides an organic cation that stabilizes the anatase polyanionic cores formed in this medium. These anatase clusters are organized so as to favour self-assembly into intermediate nanocrystals, which, in turn, self-assemble into superlattices. This self-assembling process has been exploited for the processing of highly structured titania films. Furthermore, larger anatase TiO_2 nanocrystals of different sizes and shapes have been obtained by adjusting the relative concentrations of titanium alkoxide and Me_4NOH, the reaction temperature, and the pressure. HRTEM, XRD, and EXAFS have been used to characterize the various samples and to elucidate the growth of titania anatase. Our observations are in accordance with theoretically predicted condensation and growth pathways. The formation of mesoscopic structures through a self-assembling process of the multiply charged polytitanate anions in the presence of Me_4N^+ is also discussed.

Introduction

The chemistry of titania has been the subject of much scientific and technological attention. This material is used as a white pigment in making paints and cosmetics, in the electroceramics industry, as a support in catalysis, and as a photocatalyst.[1,2] Nanostructuring of titania is of great interest with regard to the construction of membranes for gas-phase separations,[3] its use as a nanoporous electrode material in the development of new types of solar cells,[4] and its use as an active layer in the design of electrochromic devices.[5] Recently, TiO_2 coatings on glasses have been shown to exhibit interesting antifogging and self-cleaning properties.[6] The performance of titania in applications such as these could be optimized with specific microstructural and macrostructural control over the morphology of the material. Progress in this area depends on our understanding of the fundamental details by which chemical reactivity is related to nucleation and growth of titania. These processes need to be controlled at the earliest stages of production and arrested at the appropriate stage so as to furnish titania particles with the desired crystal structure and a well-defined size, shape, and surface structure. Furthermore, control over the surface chemistry of nanocrystals and their functionalization through the attachment of organic ligands may lead to organized assemblies[7] and provide new types of precursors for the processing of highly nanostructured titania-based materials.[8]

[a] Hahn-Meitner Institut, Bereich Physikalische Chemie, Abt. CD, Glienicker Strasse 100, D-14109 Berlin, Germany
E-mail: chemseddine@hmi.de
[b] Present adress: Atotec, Erasmusstr. 20, D-10553 Berlin, Germany

The fundamental physical properties of such nanoscale materials are of interest, since their small size and large surface area can lead to unexpected or dramatically differing properties.[9] The need for high-quality titania systems in order to achieve a quantitative understanding of size effects on the physical properties is another motivating factor in this work.[9]

In techniques such as CVD, MOCVD, and simple thermal pyrolysis, molecular precursors are allowed to react at rather high temperatures in the gas phase or as molecular solids.[10] Control over particle size, size distribution, shape, and crystalline orientation is inherently difficult to achieve. In contrast, in wet chemical methods, a solvent is used as the reaction medium or vehicle, and the reaction is performed at low temperature. There are many advantages in using wet chemistry for the synthesis of nanomaterials.[7] Reaction, nucleation and growth can be easily monitored and influenced. The growth can be arrested by controlling the stoichiometry or by using appropriate ligands.[11] In contrast to growing clusters on solid substrates or in solid matrices, in the liquid phase the mobility and dynamics of the growing phase is assured, allowing structural arrangement of the core and growth termination by surface restructuring and capping. By variation of the synthesis conditions or reactants and characterization of the materials obtained, the production of nanocrystals can be rationalized.[11,12] Nanocrystals can be isolated according to size in the form of soluble, processable, manageable powders, or used as precursors in the processing of films.[13]

Furthermore, a major line of development of this chemistry concerns the spontaneous generation of well-defined architecture by the self-assembly of suitably designed and functionalized nanocrystals.[7] This issue of ordered nano-

  1434–1948/99/0202–0235 $ 17.50+.50/0

structured arrays of functional nanocrystals is of central importance for the evaluation of the competitiveness of wet chemistry, i.e. sol-gel processes or solution techniques, since through the size, shape, and organization of particles, organic species can be confined within well-defined inorganic structures, allowing control over their thermal removal.[8,14] One of the problems encountered in making titania is the high reactivity of the available precursors, such alkoxides or chlorides, toward water.[15] The reaction invariably leads to a mixture of different polymeric species, which assume a variety of structures and sizes, and finally to an amorphous solid. Although certain chemical modifications have been successful in controlling the reactivity of titanium alkoxides and have permitted the isolation of intermediate polyoxoalkoxides,[16,17] none of these species resemble the structure of the bulk dioxide and any further hydrolysis again leads to gels and amorphous precipitates. In both cases, a peptization process is required to convert these polymers into crystalline particles. Control over size, size distribution, and shape is difficult during these dissolution-growth processes.[3] The present approach involves performing the reaction in a purely aqueous medium in the presence of a base, so as to achieve a complete hydrolysis and to provide conditions similar to those used in the aforementioned peptization process. Thus, hydrolysis and polycondensation of titanium alkoxide [$Ti(OR)_4$] is performed in the presence of tetramethylammonium hydroxide (Me_4NOH). This base both catalyzes the reaction[15,17] and provides an organic cation that is known to stabilize polyanionic cores in basic media, e.g. polyanions of tungsten, molybdenum, and vanadium.[18]

Results

Figure 1 shows an overview image of titania nanocrystals from a first sample, denoted as sample A. The nanocrystals are uniform in shape and are not aggregated. The particles are single nanocrystals and exhibit a triangular prismatic shape with a relatively narrow size distribution. The high resolution micrograph clearly shows lattice planes. All images of sample A show particles with an interplanar distance of 3.52 Å in the tetragonal [101] planes, which corresponds to the anatase phase. The lateral dimensions of the particles can be estimated by counting the number of lattice planes (about 30 LP in this case, which amounts to 10.5 nm). The average length measured directly from the micrograph is about 20 ± 1 nm. A careful analysis of the particles reveals structural features that can be utilized for the study of surface morphologies of small particles and the changes that occur during growth. Thin edges of TEM samples represent surfaces that can be viewed in profile by HRTEM.[20] The steps on the particle edges are in the [101] crystallographic directions and the height of each step can be taken as an indication of a cluster-cluster growth (see below). The triangular shape is in fact due to the presence of stepped [101] surfaces.

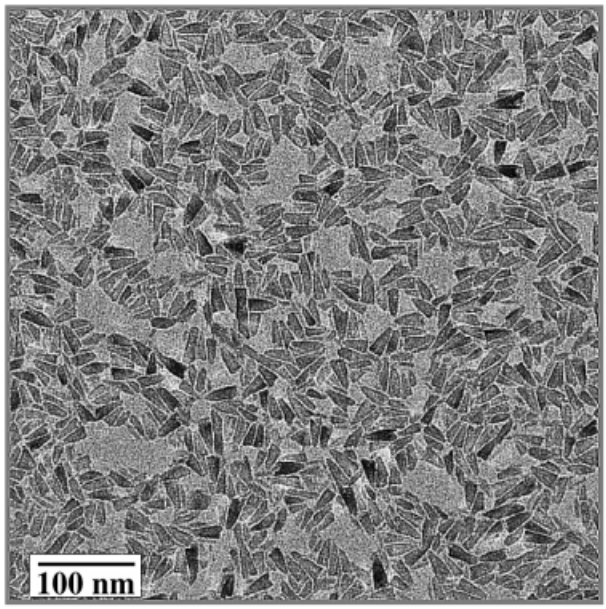

Figure 1. TEM micrograph of TMA-capped TiO_2 particles obtained for $R = 3$; the particles are homogeneous in size and triangular in shape

The X-ray diffraction pattern (Figure 2b) of sample A confirms the single anatase phase. However, all the Bragg peaks are relatively broad due to the finite size of the nanocrystals. The sizes calculated from the half-widths of the peaks using the Scherrer equation amount to 11.1 nm for the [101] peak, 20.8 nm for the [004] peak, and 20.7 nm for the [200] peak. These values are in accordance with the lateral dimensions measured from the TEM micrographs of these triangular prismatic nanocrystals.

Autoclaving of solution A leads to a shape transformation from triangular to rectangular particles, which have lengths of about 28 ± 3 nm and widths of about 12 ± 2 nm (Figure 3). The autoclaving leads to nanocrystals of uniform shape, which are non-aggregated and conform to a single anatase phase, according to TEM and XRD analysis. The morphological transformation of particles can be attributed to the thermal decomposition of the organic cations under the autoclaving conditions. The loss or decomposition of the organic cations probably induces chemical etching, which is followed by further growth and elimination of steps, ultimately leading to a shape transformation from triangular to rectangular.

Figure 4a shows a typical TEM image at low magnification of titania particles obtained in the case of sample B. A homogeneous fibrous or rod-like texture is achieved, although a relatively marked polydispersity in terms of length and width is apparent. Figure 4b shows a high-resolution image of a selected titania nanocrystal from sample B. The nanocrystal is viewed along the [010] direction. The surface profile image of the nanocrystal B shows stepped terraces on the [101] surface, which are marked with arrows. Its height is measured as a multiple of 3.52 Å, in accordance with the $d_{[101]}$. The corrugated sides are structural features that have not previously been observed in the case of titania

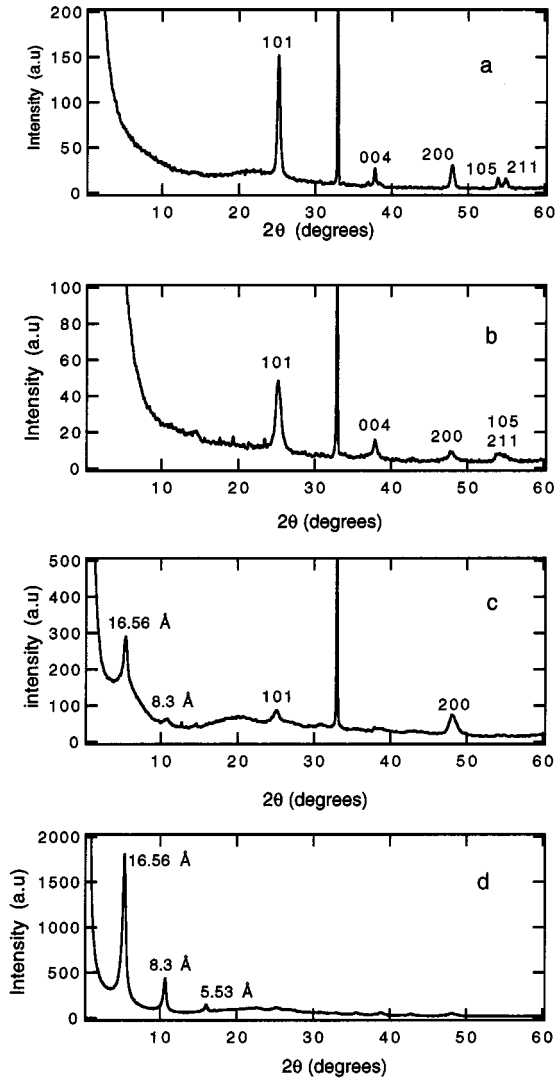

Figure 2. X-ray powder diffractograms of TiO_2 nanocrystals made with various Ti/Me_4N^+ ratios *R*; Figures b, c, and d correspond to solutions A ($R = 4$), B ($R = 1.25$), and E ($R = 0.84$); Figure a was obtained after autoclaving solution B under a saturated vapor pressure of water at 200°C and 2500 kPa; large-angle peak assignments are based on anatase titania; peak broadening indicates a decrease of nanocrystal size with increasing *R*; in addition to the perfect organization in the lateral dimensions shown in Figure 10, the series of harmonics in d indicates ordering of the growing anatase cluster in the nanocrystals forming a layered nanostructure; the sharpness of the peaks indicates a high degree of structural communication between the nanocrystals

and are a consequence of cluster-cluster growth and condensation of skewed octahedra in the case of anatase (see Discussion). The two sets of lattice fringes give two interplanar distances, which correspond to the [101] and the [002] of the anatase crystal structure (Figure 5). The elongated particles lie in the [010] plane.

XRD measurements on films obtained by the deposition of sample B solution onto a silicon wafer (Figure 2c) yield further information on the polydispersity of the sample. The low-angle peaks correspond to the presence of smaller titania clusters (cf. sample E). The relatively high intensity of the [200] peaks compared to the [101] peak is indicative

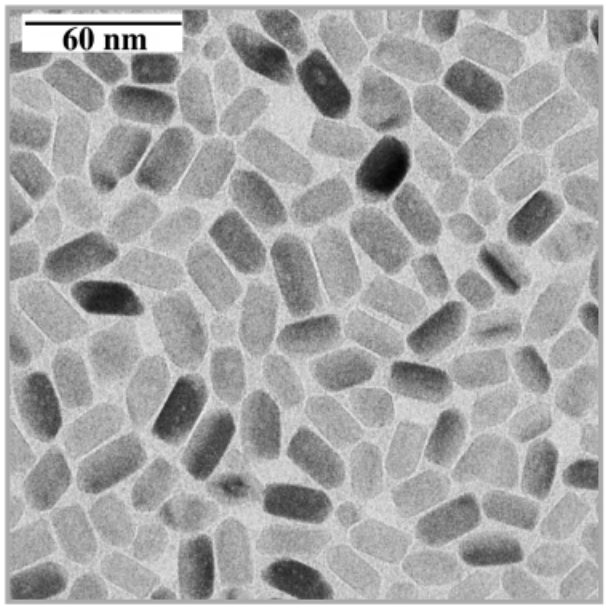

Figure 3. Overview of titania nanocrystals prepared by autoclaving solution A; the nanocrystals are homogeneous in both shape and size

of film anisotropy and confirms a preferred orientation of the crystallites. The Scherrer equation leads to 92.9 Å for the [101] peak and to 79.6 Å for the [200] peak.

Figure 6 shows TEM images of particles obtained after autoclaving sample B. The rod-like morphology is maintained. The diameter of the rods varies between 15 and 20 nm, but a large polydispersity in terms of rod length is apparent ($76 < L < 177$ nm). The adopted procedure of adding the titanium alkoxide solution in a dropwise fashion is mainly responsible for the observed polydispersity. In contrast to sample A, where a shape transformation was seen to occur, further growth in length and diameter takes place during the autoclaving of solution B without a change in the rod-like morphology. However, the structural features on the surface, such as sharp edges and steps, are no longer present. Again, the surface reconstruction can be related to the thermal decomposition of the organic cations under the autoclaving conditions. This confirms the role of the Me_4N^+ cation as a good capping ligand in stabilizing the surface structure of titania nanocrystals.

The size of the particles can also be fine-tuned by changing the autoclave temperature. Autoclaving of portions of sample B at 175°C and 200°C for a duration of 5 h resulted in particle sizes, calculated using the Scherrer equation, of 18 nm and 12 nm, respectively, for the [101] peak, and of 15.6 nm and 14 nm, respectively, for the [200] peak. The average width of nanocrystals measured from the TEM images is of the same order (about 12.32 nm). The average length of 63 nm reflects the nanocrystal dimension in the [002] direction, as shown in Figure 6b.

As mentioned above, the adopted procedure of adding the titanium alkoxide solution in a dropwise fashion accounts for the observed polydispersity in samples A and B. Figures 7a and 7b show two typical images obtained from

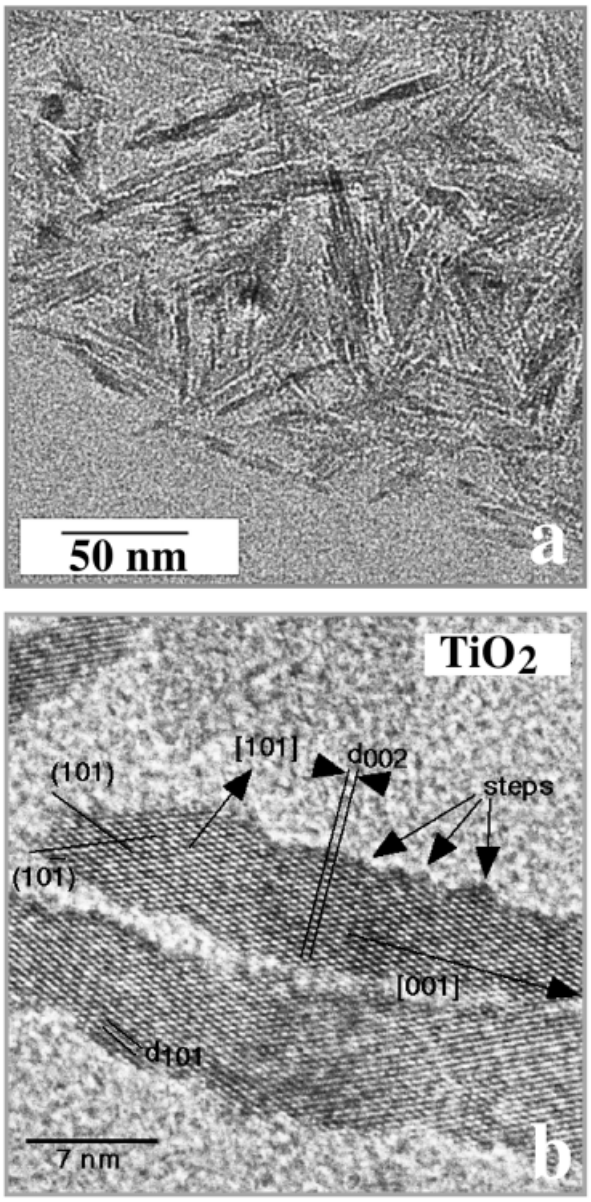

Figure 4. a) Elongated nanocrystals prepared with $R = 1.25$ (solution B); b) HRTEM of nanocrystals lying in the [010] plane and elongated in the [001] direction; the corrugated sides shown by arrows are due to oscillatory repetition of [1 0 1] and [1 0 −1] planes

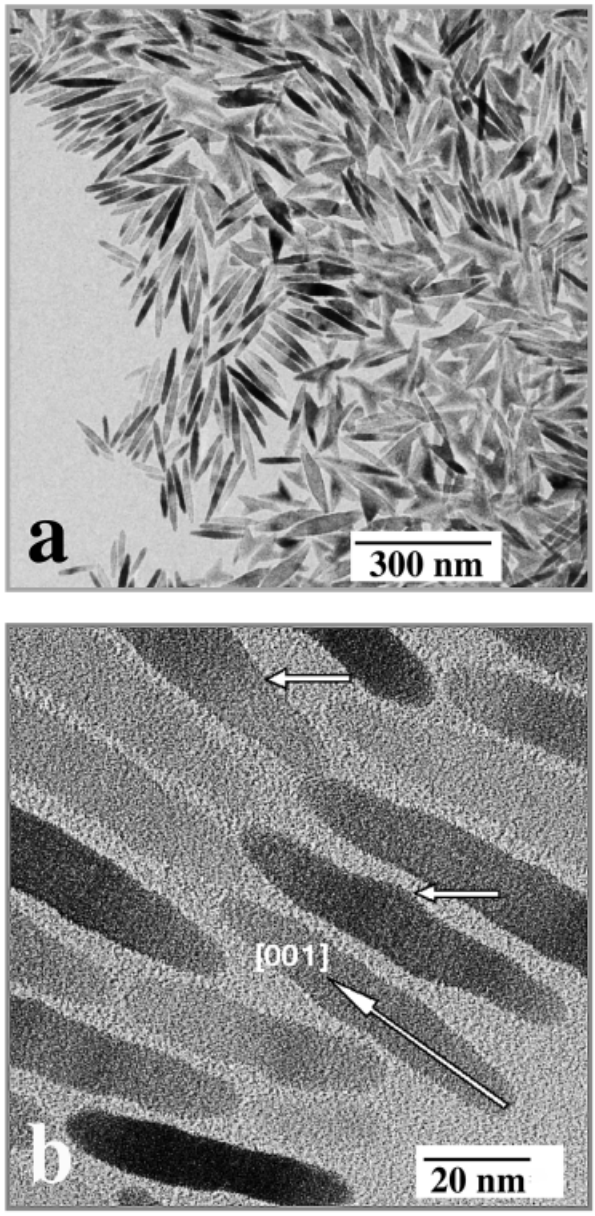

Figure 6. a) Overview of nanocrystals obtained after autoclaving B at 200°C, 2500 pKa for 5 hours; b) HRTEM shows no sharp edges and no clear surface steps after NMe_4^+ decomposition

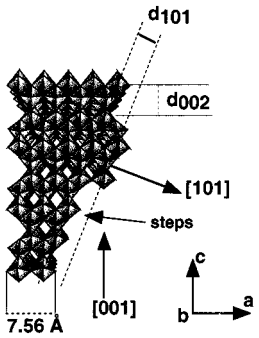

Figure 5. Polyhedral and packing drawing of anatase, TiO_2 in the [010] projection; [101] and [001] growth directions and a stepped [101] surface are shown

sample C ($Ti/Me_4NOH = 2$), made by adding the titanium alkoxide solution in a single portion. The sample has a relatively homogeneous appearance at low magnification. Particles of two distinct shapes are formed. These two particle types represent unique morphologies, in the sense that they are themselves the products of a self-assembling process (aggregation) of smaller elongated titania particles (slabs), as indicated by arrows in Figure 7b.

Particles with a triangular prismatic shape are also present in sample C, as indicated by arrows in Figure 7a. In contrast to sample A, where the particles are single nanocrystals, particles in sample C are composed of smaller ti-

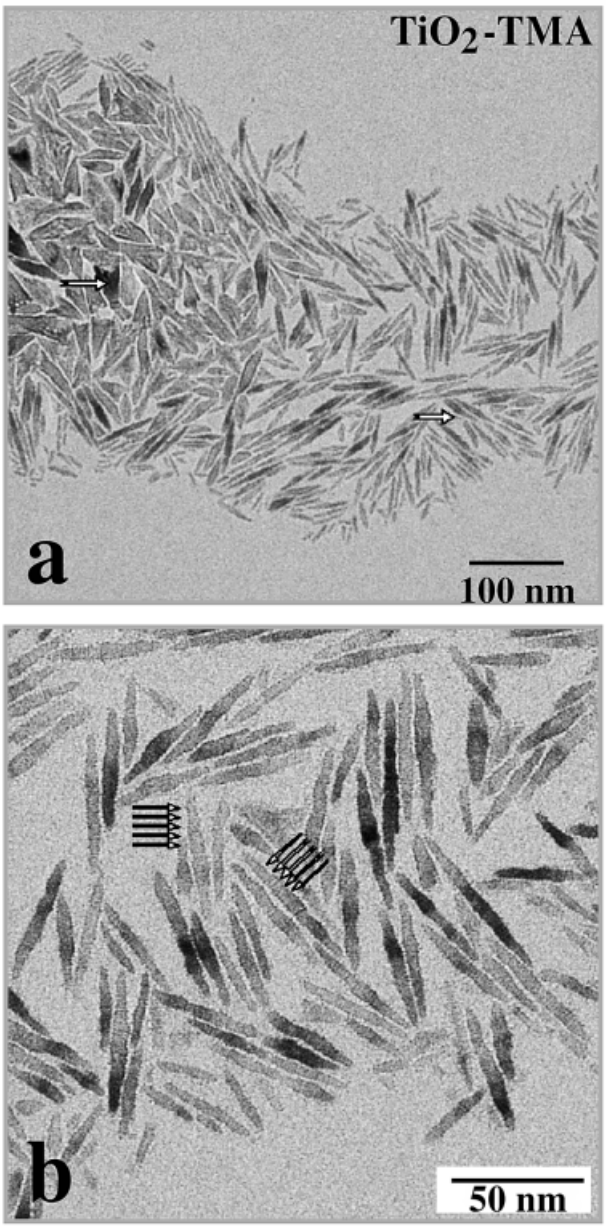

Figure 7. a) Two type of particles, shown by arrows, are obtained in solution C; b) These particles are composed of self-assembled smaller slabs as indicated by arrows

tania particles (slabs) self-assembled into aggregates of triangular shape.

Figure 8 shows images obtained from sample D (Ti/Me_4NOH = 1). At low beam intensities, the particles exhibit an internal structure as that in the case of sample C. Slabs are disposed parallel to one another along the [001] direction. At high magnification (higher electron fluxes), a coalescence (condensation) is induced by the loss of the organic cations (see Figure 8). The nanocrystals are viewed along the [010] axis, oriented parallel to the electron beam. The coalescence of these slabs (building units) leads to particles with corrugated sides or stepped [101] surfaces, as shown by black arrows in Figure 8. In addition to these thin slabs, as already observed in the case of sample C, spherical particles are formed. Particles of this type form at R = Ti/$Me_4NOH \leq 1$ and they show a propensity to self-assemble into organized structures. Their concentration increases, at the expense of their elongation, with the TMA concentration.

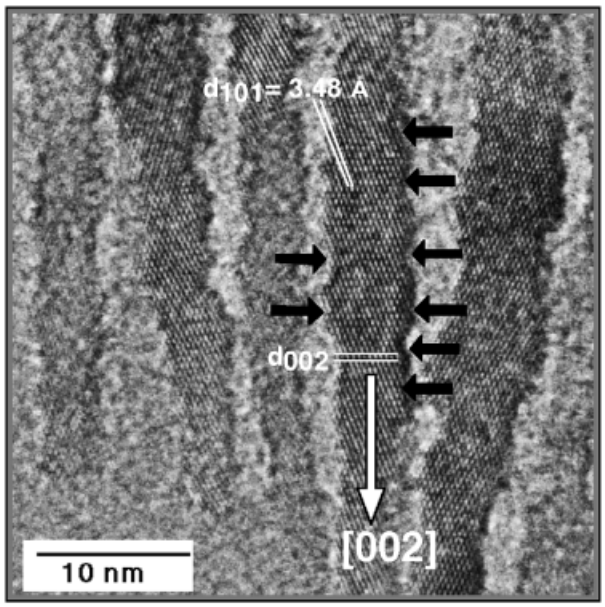

Figure 8. Titania clusters made in solution D; elongated slabs self-assemble into aggregates; at high magnification (higher electron fluxes) the particles coalesce into elongated nanocrystals presenting the same corrugated sides shown by arrows

Figures 9a and 9b show TEM images obtained in the case of sample E. The particles are seen to be organized in an ordered structure (2D superlattice). TEM provides a real-space imaging of the superlattice. In addition, small-angle electron diffraction can be used to probe the superlattice structure on the micrometer scale, while small-angle XRD allows insight into the structures of individual titania/Me_4N^+ nanocrystals on the Ångström scale. Figure 9 shows an array of nanocrystals with a mean inter-particle (center-to-center) distance of 15.7 nm, determined by direct imaging and confirmed from the power spectrum. The high magnification Figure 9b reveals well-faceted hexagonal crystals that form a hexagonal close-packed sheet. The crystals measure 13.5 nm in diameter. The high regularity in terms of size and shape, and long-range translational and orientational order is confirmed by the relatively sharp spots seen in the power spectrum (see inset in Figure 9a).

Further structural information is provided by X-ray diffraction (XRD). Measurements performed on thin films obtained by solution deposition on various supports, particularly on silicon wafers, are very sensitive to the periodicity perpendicular to the substrate (Figure 2d).

The diffraction intensity appears in two distinct scattering regions, the small-angle and large-angle. A series of harmonics at inter-plane distances of 16.56, 8.3, and 5.53 Å indicates an orientation in the direction normal to the substrate. The titania clusters are stacked in columns directly on top of one another, forming a multilayered struc-

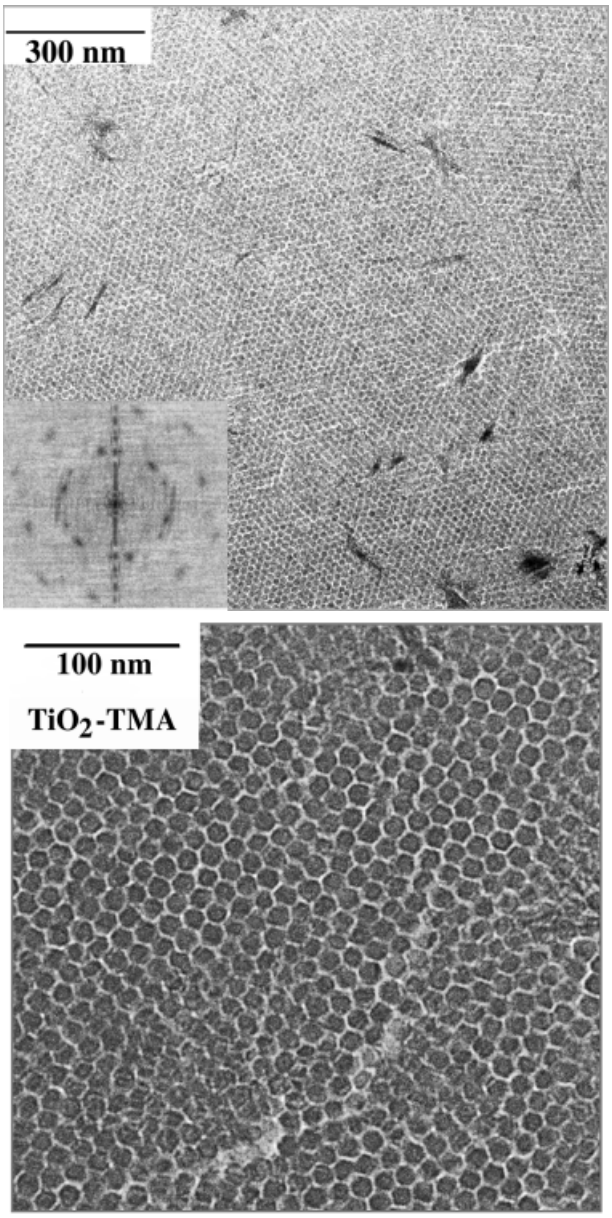

Figure 9. a) Transmission electron micrograph of titania/Me_4N^+ nanocrystals self-assembled into a superlattice with dimensions of the order of μm; the power spectrum (inset) confirms the long-range translational and orientational order of the superlattice; b) high magnification shows well-faceted hexagonal nanocrystals

ture. The majority of the nanocrystallites have the same orientation of their layered structures, which accounts for the sharpness of the XRD peaks.The white space observed around the nanocrystals in Figure 9 is probably occupied by organic cations.

Figure 10 shows TEM images of particles obtained in the case of sample F, which corresponds to solution E kept under reflux for an additional hour. The arrays obtained exhibit less regular geometries on a large scale. In comparison with sample E, changes in particle shape and in their organization, as well as in the internal structures of the nanocrystals are observed. Instead of the hexagonal shape observed in E, the drying leads to a rectangular shape and the nanocrystals are differently packed (Figure 10). Furthermore, two types of internal structures are observed. This can be explained in terms of the presence of two competing structures, since one type of nanocrystal is seen to be composed of slabs disposed parallel to one another, while the other type does not have any discerning features. Another explanation is that in a few nanocrystals a condensation process takes place, leading to slabs. These local transformations will affect the self-assembling process, thereby leading to new structures. A very interesting observation is that the high magnification images reveal that the newly formed slabs adopt a zig-zag structure. This is an indication of the presence of *cis*-skewed chains, characteristic of the anatase crystal structure (Figure 10). In fact, these anatase slabs are the condensation products of smaller ones (sample E), the anatase structure of which was shown by EXAFS and XRD experiments.

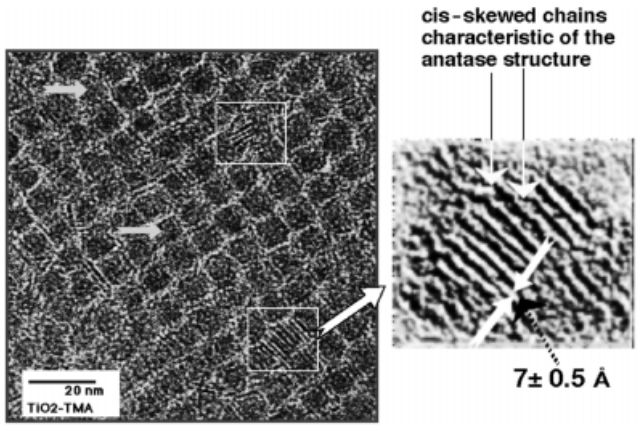

Figure 10. Nanocrystals obtained from solution F: Arrow shows nanocrystal composed of slabs disposed parallel to one another; high magnification indicates structural features that can be related to the *cis*-skewed chains in the [001] direction of the anatase crystal structure; the neighboring nanocrystals do not exhibit the same internal structure; arrows point to small clusters that probably did not condense to give slabs; a competing structure, where the slabs are differently oriented, is present

Figure 11 shows particles obtained in the case of sample G, using the same composition as in sample D, but with $(C_5H_{11})_4NOH$ as the base instead of Me_4NOH. The particles obtained are also elongated and relatively homogeneous, with widths of about 3.6 nm and lengths of about 42 nm. The important difference is the absence of the corrugated sides observed with Me_4N^+. The sharp edges indicate a relatively flat [100] surface. High-resolution microscopy shows most particles to be single nanocrystals, and a structural regularity where only [101] lattice planes are observed for most particles. The use of $(C_5H_{11})_4N^+$ illustrates the influence of cation size on the growth of titania, the larger ion leading to [100] surfaces instead of [101] surfaces.

Figure 12 depicts an electron micrograph of particles of sample H. The particles are almost spherical in shape and display a large size distribution (102 nm < diameter < 5 nm). Besides the spherical particles, a few elongated forms (or slabs) are also present, as indicated in Figure 12. By

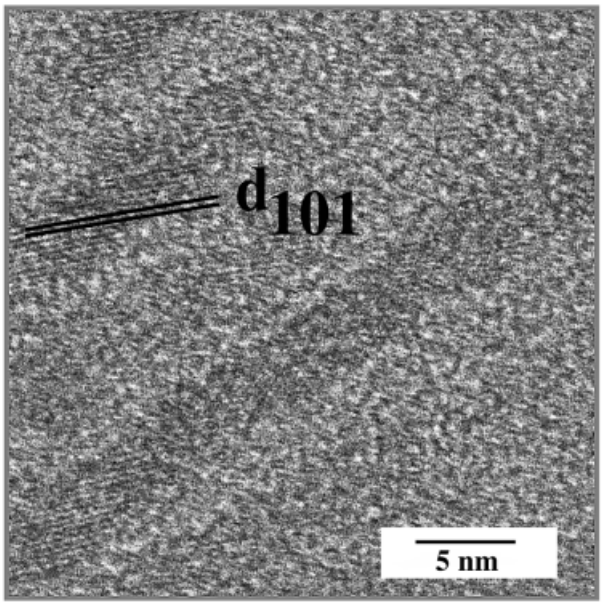

Figure 11. Elongated nanocrystals made with TPA; HRTEM showing no corrugated sides but relatively sharp edges corresponding to flat [100] surfaces

comparison with sample E, this experiment shows the importance of stirring with regard to the size distribution of particles.

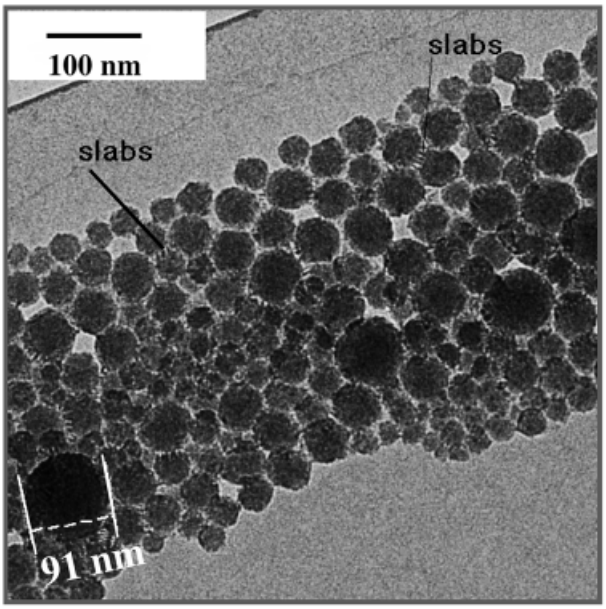

Figure 12. Overview of nanocrystals obtained without continuous stirring; in addition to the wide distribution of sizes, some slabs are observed (arrows), which seem to bridge or to interact with neighboring spherical nanocrystals

Figure 13 shows particles of sample I, made using the same procedure as in the case of sample E but with titanium tetrabutoxide Ti(O*n*Bu)$_4$ as the titanium source in butanol. The particles are almost spherical in shape and display a very narrow size distribution, having a mean diameter of about 7 nm. In this overall view of the particles, some small organized domains can be observed. However, no long-range order is apparent. The difference in size and shape of the particles compared to those in sample E can be attributed to the nature of the alkoxide groups.

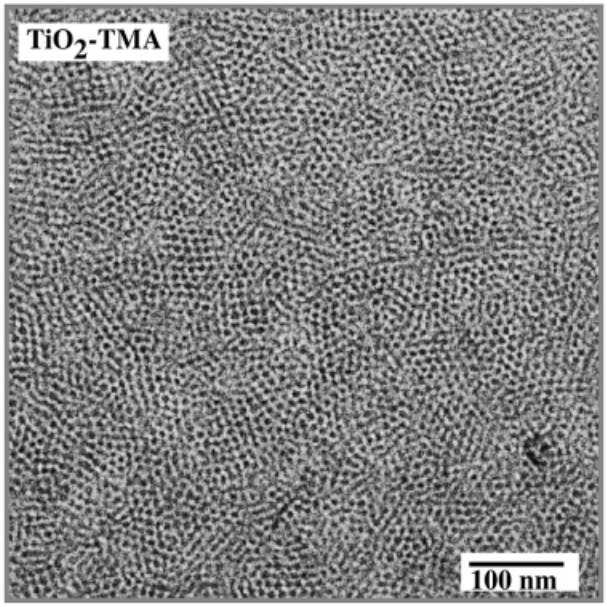

Figure 13. A new type of nanocrystal is obtained with titanium tetrabutoxide in butanol; monodisperity is achieved but the nanocrystals are smaller compared to those in sample E

Sample J was prepared using a 10-fold more concentrated titanium alkoxide solution. The condensation products are titania fibres or slabs of uniform width (7.5 ± 1 Å). However, polydispersity in slab length is in evidence (1 < *L* < 18 nm), as can be seen in Figure 14.

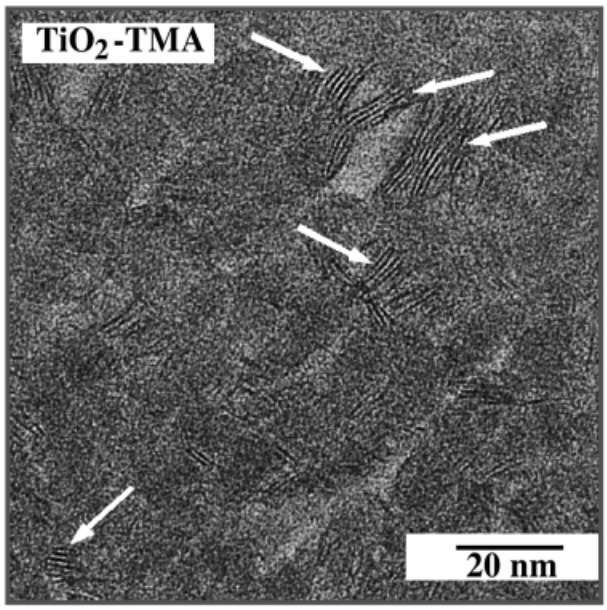

Figure 14. A further increase in titanium concentration leads to the formation of longer and relatively stable slabs, or of polymers with a polydispersity in length; the same width is observed for all polymers

Discussion

As far as we are aware, the work reported herein represents the first incidence of the tailoring of the morphologies of titania nanocrystals with the anatase crystal structure under homogeneous conditions by variation of the hydrolysis conditions and control of the hydrothermal treatment. In this approach, relatively high concentrations of the alkoxide [$Ti(OR)_4$] are used. The hydrolysis is performed in the presence of excess water and a base is employed to catalyze the complete hydrolysis of all OR groups. The effects of unhydrolyzed OR groups on the condensation pathway or on the structure of the primary polycondensed species are therefore avoided. Moreover, hydrolysis and condensation are not separated due to the high titanium concentrations.[17] This methodology leads to a totally new type of clusters and nanocrystals, exhibiting exclusively the anatase crystal structure, with stabilization by tetramethylammonium cations (Me_4N^+).

The hydrolysis and condensation of titanium alkoxide or titanium cations in solution has been the subject of a great deal of attention.[17,21] Particularly relevant to the present results is the theoretical work based on the partial charge model by Henry and Livage, developed to understand and predict inorganic polymerization in the case of transition metal oxide precursors,[21] as well as the work by Bradley on the hydrolysis of titanium alkoxides in the presence of a base.[22] According to these authors, the presence of a base influences the condensation by favouring the formation of the highly nucleophilic TiO^-. This reactive condensation precursor reacts with the positively charged titanium, leading to the formation of polymeric materials.[17]

In the case of a highly dilute alcoholic solution of the alkoxide, the overall hydrolysis reaction after the addition of excess water can be written as:

$$Ti(OR)_4 + 4\ H_2O \rightarrow Ti(OH)_4 + 4\ ROH \quad (a)$$

However, at the high titanium concentrations used in the present study, it is difficult to separate the hydrolysis (Equation a) and condensation (Equation b) processes. These two primary processes are accelerated by the presence of Me_4NOH as a result of the formation of the highly nucleophilic TiO^- according to Equation c. The cation also plays a role in preventing further condensation and stabilizing condensed species according to Equation d.

$$Ti{-}OH + XO{-}Ti \rightarrow Ti{-}O{-}Ti + XOH\ (X = H, R) \quad (b)$$
$$Ti{-}OH + Me_4NOH \rightarrow Ti{-}O^- + Me_4N^+ + H_2O \quad (c)$$
$$Ti_xO_yH_z + Me_4NOH \rightarrow (Ti_xO_yH_{z-1})Me_4N + H_2O \quad (d)$$

The Me_4NOH concentration will also determine the *x* and *y* values and therefore the size of the condensed species. According to refs.[17][22] reaction according to Equation c leads to polymers, which is consistent with the formation of stable polymeric material in Figure 14, or of slabs in Figure 7b. In terms of the partial charge model,[21] the formation and stabilization of a totally new type of clusters, slabs, polymers, or nanocrystals, exhibiting exclusively the anatase crystal structure, can be explained by considering a condensation process dominated by an olation pathway, which is seemingly favoured under the present experimental conditions.[17][21] It is generally accepted that early in the condensation process, the coordination number of titanium changes from 4 to 6, and that the basic building unit in the polymerization process is an octahedral arrangement of six oxygen atoms around a titanium centre.[17][21] These octahedra link together by sharing edges, so as to form dimers. According to the partial charge model, these dimers condense to form skewed chains as a result of olation processes, as illustrated in Figure 15.[21] In the presence of Me_4N^+, the condensed species can be stabilized allowing their isolation, or may be forced to condense into larger particles by further heat treatment. In the early stages of condensation, the linear growth (polymerization) leads to skewed chains,[21] which corresponds to growth in the [001] direction of the anatase phase (main stem). Then, through an oxolation process, the nuclei can grow in one of the two equivalent directions.[21] The shape of the particle will be determined by the difference in growth velocities in the [101] and [001] directions, as indicated in Figure 5. At low concentrations of Me_4N^+, growth is favoured in the the [101] direction (Figure 1), while at high concentrations the growth velocity is favoured in the [001] direction (Figure 4). Therefore, the shape of nanocrystals can be fine-tuned by changing the ratio Ti/Me_4NOH, denoted as *R*.

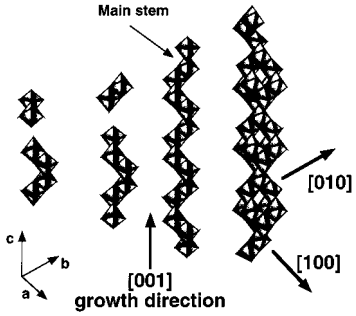

Figure 15. Model to explain condensation and growth of titania anatase; the mode of linking dimers imposes restriction on the growth direction leading to *cis*-skewed chains (main stem) and this is favoured by the physicochemical conditions of the present reaction; [100] and [010] are the first branching directions; then, depending on the organic cation present and its concentration, the secondary branching can be parallel to [101] or can remain parallel to [100] and [010]

The HRTEM micrograph shown in Figure 4b and the illustration in Figure 5 relate to titania nanocrystals where the [101] and [010] are the predominant surfaces. The corrugated sides are due to oscillatory repetition of [1 0 1] and [1 0 −1]. In terms of the mechanism discussed above, the main stem of the nanocrystal is seemingly in the [001] direction. The [100] and [010] directions are equivalent in the case of the anatase crystal phase, and both can be primary branching directions. Sample B, heat-treated for only 2 h, was found to contain small slabs and very thin elongated particles in the [001] crystallographic direction; in Figure 1 nanocrystals also show stepped [101] surfaces. The surface steps are of a height equivalent to the cluster size. Growth

will take place by the building-up of these steps so as to form new cluster layers, and the rate of this process will depend on the concentration of Me_4N^+. The crystal surface in contact with the building units can be influenced by Me_4N^+. This cation seems to interact preferentially with the [101] surface, leading to the favoured development of these surfaces, as shown in Figures 4b.

The decomposition of Me_4N^+ at higher temperatures and pressures leads to surface reconstruction and further growth. The structural features observed on the surface, such as steps, corrugated sides, and sharp edges are, in fact, stabilized by Me_4N^+. However, no corrugated sides or steps are observed in the presence of $(C_5H_{11})_4N^+$ cations (Figure 11). The [100] surfaces of the particles are relatively flat. The observed effect of cation size on nanocrystal shape can be explained in terms of the role of the cations during the early stages of condensation, and thereafter during the crystal growth. Preliminary attempts to stabilize smaller clusters by replacing Me_4N^+ with $(C_5H_{11})_4N^+$ were not successful.

The Me_4N^+-stabilized clusters are able to self-assemble to form nanocrystals, which can be identically replicated in unlimited quantities provided that vigorous stirring of the solution is maintained during the hydrothermal reaction (see Figure 9, and to some extent Figures 10 and 13 as well). Without stirring, a wide size distribution is generally obtained, as shown in Figure 12, where arrows indicate the additional presence of slabs. In fact, the monodispersity of the primary clusters determines the monodispersity of the intermediate nanocrystals formed by a self-assembling process and, therefore, the formation of the superlattice observed in Figures 9 and 10. These results clearly indicate the construction of a superlattice in 3 steps. This was called a progressive condensation process in our preliminary report.[23] The overall process first involves the formation of the monodispersed primary building units. Secondly, they self-assemble into nanocrystals with a diameter of 13.5 nm. Finally, these nanocrystals are made to self-assemble in a uniform manner to form a superlattice. These clusters and nanocrystals are negatively charged and their electrostatic repulsion accounts for the stability of the solutions inasmuch as it prevents flocculation. On the other hand, these interactions and the monodispersity are responsible for the long-range ordering observed after evaporation of the solvent (Figure 10). The charged titania nanocrystals are aligned in a periodic array, rather like in a crystal.[24]

The very broad peaks seen in Figure 2d and the preliminary EXAFS experiments performed on our samples, particularly on sample E, are indicative of the anatase crystal structure.[25] The structural changes observed after an additional heat-treatment of E to make F clearly indicate a further condensation among a few nanocrystals to form slabs, with the *cis*-skewed chains being characteristic of the anatase crystal phase. Further structural information could be gleaned from the XRD pattern of cluster films prepared by simple deposition of solution E onto a silicon wafer followed by drying in air (Figure 2d). A similar procedure was used to obtain TEM measurements, where one drop of the solution was applied to a carbon film. A series of peaks at low angular range with the spacings 16.56 Å, 8.3 Å, and 5.53 Å was observed, attributable to [001], [002], and [003] reflections, respectively, of a spacing of 16.56 Å. These XRD data suggest that the clusters are arranged inside the nanocrystal such as to form a layered structure. Packing of this type has been observed in the case of colloidal nanosheets made from exfoliated titanate. The exfoliation/reassembly process in the presence of tetrabutylammonium hydroxide Bu_4N^+ leads to a comparable XRD pattern.[26] In both cases, drying of the aggregate leads to textured films, in which reflections are suppressed due to the preferred orientation of the nanosheets or, in this case, clusters or slabs. The thickness of the nanosheets is 7.5 Å, which is comparable to the thickness of the slabs (sample F), while their lateral dimension is in the range 0.3−1 μm.[26] Figure 10 shows nanocrystals composed of slabs disposed parallel to one another with a repeating distance of about 16 ± 1 Å. This distance falls within the range of the spacings estimated from the XRD pattern of sample F, which is analogous to Figure 2d.

The observed stepped surfaces in Figures 1 and 4b give indications of a cluster-cluster growth of titania anatase nanocrystals, especially the corrugated sides observed in the case of sample B. According to XRD, these particles are already formed at the reflux stage, i.e. in solution. In the case of samples C and D, particles are seen to be composed of aggregated small slabs at low magnification, which subsequently coalesce into elongated particles also having corrugated sides (Figure 8) like those of sample B grown in solution (Figure 4). This direct observation suggests that a cluster-cluster growth takes place in solution. The coalescence process that takes place under the electron beam still has to be carefully investigated.

The nature of the intermediate nanocrystals observed in Figure 9 proved to be sensitive to the OR group of the alkoxide. Figure 13 shows smaller nanocrystals formed when titanium tetrabutoxide in butanol was used (particle diameter ca. 8−9 nm). The difference in size, and probably in the internal structure as well, highlights the importance of the OR group in the hydrolysis and condensation processes.

The ordering observed in Figure 9 is due to electrostatic interactions between the multiply charged titanium polyanions and the Me_4N^+ cations and leads to intermediate nanocrystals. In turn, through inter-nanocrystal interactions, these form a long-range ordered array, comparable to arrays of pores typically observed in mesophases. In the case of polysilicates, the self-assembly process can be accompanied by a condensation-polymerization process, leading to the formation of three-dimensionally structured arrays, which are stable even after calcination.[27,28]

The present synthetic technique furnishes titania clusters of various sizes and shapes in solution. These clusters may be used to grow transparent thin films, allowing control over both the orientation of superlattices and that of individual nanocrystals. The exact internal structure of the superlattice still has to be determined, and this will be addressed once single crystals are obtained. However, EXAFS

results, XRD, HRTEM, and elemental analysis indicate the presence of anatase clusters and Me_4N^+ cations. Optical measurements and X-ray photoelectron spectroscopy (XPS) indicate dramatic changes in the electronic properties of the titania nanocrystals according to their size and shape.[25]

Conclusion

We have presented a new method for preparing titania nanocrystals with exclusively the anatase crystal structure. Small titania clusters or polytitanate anions have been prepared and stabilized in solution for the first time. Cluster-cluster growth has been shown to take place, leading to larger nanocrystals. The growth can be influenced by controlling the hydrolysis and condensation with Me_4NOH. There is an apparent preference for interaction between [101] surfaces and Me_4N^+, which would account for the differential growth velocities in the [101] and [001] directions. The monodispersity of the negatively charged clusters renders them suitable for the progressive formation of titania/Me_4N^+ superlattices. Thin-film growth allows control over the orientations of superlattices, individual nanocrystals, and individual clusters. The polycondensation and growth processes observed and discussed in this study are in accordance with theoretical predictions. These new results should motivate further investigations of titania and polytitanates in solution.

Experimental Section

General: All hydrolysis reactions were conducted in air, whereas the refluxing of solutions was carried out under argon.

Chemicals: All chemicals used were analytical grade or of the highest purity available and were used as purchased. 2-Propanol and butanol from Merck; titanium isopropoxide $Ti(OiPr)_4$ and butoxide $Ti(OnBu)_4$ from Aldrich, and tetramethylammonium hydroxide Me_4NOH and tetrapentylammonium hydroxide $(C_5H_{11})_4NOH$ from Fluka.

Synthesis of TiO_2 Clusters and Nanocrystallites: A 250-mL three-necked flask was placed in a large crystallizing dish on top of a magnetic stirrer, and the side necks were fitted with a thermometer and a gas inlet tube. A magnetic stirrer bar and 150 mL of aqueous Me_4NOH solution were placed in the flask and the crystallizing dish was filled with ice. When the temperature of the Me_4NOH solution had reached 2°C, a solution of 0.333 mL of titanium isopropoxide in 10 mL of 2-propanol was added dropwise by means of a dropping funnel (1 drop/s) while the mixture was stirred vigorously. During the course of the addition, a white precipitate formed. After the addition was complete, the mixture was left to stand for 10 min, then the ice bath was replaced by a heating mantle, and the mixture was heated. On refluxing, the precipitate dissolved after about 3 h, but after 6 h the solution became slightly turbid once more (sample A).

Sample B was prepared according to the same procedure, but using different concentrations (see Table 1); the mixture became slightly turbid only after all the titanium alkoxide solution had been added (about 5 min). In this case, aliquots were withdrawn from the refluxing solution after 2 h and 6 h in order to carry out TEM observations.

Aliquots of solutions A and B (8 mL each) were heat-treated in a titanium autoclave at 175 and 200°C for a period of 5 h under a saturated vapor pressure of water (about 2500 kPa) in a titanium-coated reactor.

For the preparation of all other samples, the procedure adopted was similar to that described above, except that the titanium alkoxide solution was added in a single portion rather than dropwise to the Me_4NOH solution (see Table 1).

Table 1. Stoichiometry of the reactions

Sample	$Ti(OR)_4$ x µmol[a]	Me_4NOH y µmol[a]	Reflux [h]	Temperature [°C]
A	1.14	0.26	6	90−100
B	1.14	0.82	6	90−100
C	1.14	0.57	6	90−100
D	1.14	1.09	6	90−100
E	1.14	1.36	6	90−100
F	1.14	1.42	7	90−100
G	1.14[b]	1.17	6	90−100
H	1.14	1.36	13 d	50−60
I	1.06[b]	1.42	6	90−100
J	11.4	11.6	6	90−100

[a] x µmol of titanium isopropoxide in 10 mL of 2-propanol, y µmol of Me_4NOH in 150 mL of water. − [b] Sample G was prepared with tetrapentylammonium hydroxide (TPA) and sample I with titanium tetrabutoxide in butanol. Sample H was left for 13 d without stirring.

Elemental Analysis of Sample E was carried out commercially at the microanalytical laboratory Pascher in Remagen-Bahndorf, Germany. Elemental analysis of powder E, dried at room temperature in air: C 18.22, H 5.5, N 4.9, O 42.87, Ti 33.3. The composition can be roughly written as $Ti_4O_{15}[N(CH_3)_4]_2H_{12}$.

Film Growth: The samples were prepared by depositing freshly prepared solutions on a silicon [100] wafer or on glass. In some cases, the solutions were first concentrated in a rotary evaporator prior to deposition in order to accelerate thick-film processing. Optically transparent films of ordered titania nanocrystals could be prepared by controlling the rate of evaporation of the solvent. Slow evaporation leads to thin film growth, which allows orientation of the superlattice and of the individual layered structures. Such deposition on solid substrates produces ordered and oriented films.

The titania clusters and nanocrystals were investigated with a Philips CM12 transmission electron microscope. Samples were prepared by placing a drop of the freshly prepared nanocrystal solution on a carbon film supported on a Cu grid. The advantages of investigating crystal growth in the case of nanocrystals is that the specimens are already thin to the point of electron transparency, and are thus readily amenable to TEM examination. High resolution is quite easily achieved nowadays and image processing is straightforward, allowing a stimulating interplay between synthesis and TEM observation.[19] A careful analysis of the micrographs can provide unique periodical and morphological information to aid in the understanding of the effects of additives on crystal growth. The NIH image-processing program was used to enhance the data obtained from some samples.

X-ray Powder Diffraction and Small-Angle X-ray Scattering were carried out with a Siemens D500/5000 diffractometer, operating with a Cu anode at 45 kV and 30 mA. A secondary graphite monochromator was used to select the K_a1 and K_a2 lines.

Acknowledgments

The authors are indebted to U. Bloeck and D. Su for technical assistance in obtaining TEM images, and to K. Diesner for performing the XRD experiments.

[1] A. Fujishima, K. Honda, *Nature* **1972**, *238*, 37−38.
[2] A. Fujishima, K. Kohayakawa, K. Honda, *J. Electrochem. Soc.* **1975**, *122*, 1487−1489.
[3] B. Kraeutler, A. J. Bard, *J. Am. Chem. Soc.* **1978**, *100*, 5985−5992; A. Chemseddine, H. P. Boehm, *J. Mol. Catal.* **1990**, *60*, 295−311.
[4] B. O. Regan, M. Graetzel, *Nature* **1991**, *353*, 737−739.
[5] C. G. Granqvist, *Handbook of Inorganic Electrochromic Materials*, Elsevier Science, Amsterdam, **1995**.
[6] R. Wang, K. Hashimoto, A. Fujishima, *Nature* **1997**, *388*, 431−432.
[7] A. Chemseddine, H. Jungblut, S. Boulmaaz, *J. Phys. Chem.* **1996**, *100*, 12546−12551.
[8] A. Chemseddine, M. L. Fearheily, *Thin Solid Films* **1994**, *247*, 3−7.
[9] R. D. Andres, R. S. Averback, W. L. Brown, L. E. Brus, W. A. Goddard, A. Kaldo, S. G. Louie, M. Moscovits, P. S. Peercy, S. J. Riley, S. J. Siegel, F. Spaepen, Y. Wang, *J. Mater. Res.* **1989**, *4*, 704−736.
[10] J. Augustynski, J. Hinden, C. Stalder, *J. Electrochem. Soc.* **1977**, *124*, 1063−1064; Y. Takahashi, A. Ogiso, R. Tomodo, K. Sugiyama, H. Minoura, M. Tsuiki, *J. Chem. Soc., Faraday Trans.* **1982**, *78*, 2563−2571.
[11] A. Chemseddine, H. Weller, *Ber. Bunsen Ges. Phys. Chem.* **1993**, *97*, 636−637; A. Chemseddine, *Chem. Phys. Lett.* **1993**, *216*, 265−269; T. Vossmeyer, L. Katsikas, M. Giersig, I. G. Popovic, K. Diesner, A. Chemseddine, A. Eychmüller, H. Weller, *J. Phys. Chem.* **1994**, *98*, 7665−7673.
[12] R. L. Whetten, J. T. Khoury, M. M. Alvarez, S. Murthy, I. Vezmar, Z. L. Wang, P. W. Stephens, C. L. Cleveland, W. D. Luedtke, U. Landman, *Adv. Mater.* **1995**, *8*, 428−433.
[13] A. Chemseddine, *Mat. Res. Soc. Symp. Proc.* **1994**, *346*, 881−886.
[14] A. Chemseddine, M. Fieber-Erdmann, E. Holub-Krappe, S. Boulmaaz, *Z. Phys. D* **1997**, *40*, 566−569.
[15] D. C. Bradley, R. C. Mehrotra, D. P. Gaur, *Metal Alkoxides*, Academic Press, London, **1978**.
[16] V. W. Day, T. A. Eberspacher, Y. Chen, J. Hao, W. G. Klemperer, *Inorg. Chim. Acta* **1995**, *229*, 391−405.
[17] J. Livage, M. Henry, C. Sanchez, *Prog. Solid State Chem.* **1988**, *18*, 259−341.
[18] M. S. Whittingham, J. Li, J. D. Guo, P. Zavalij, *Mater. Sci. Forum* **1994**, *152−153*, 99−108.
[19] R. Sinclair, *MRS Bulletin* **1994**, (June), 26−30.
[20] S. Ijima, *J. Electron Microsc.* **1985**, *34*, 249−265.
[21] M. Henry, J. P. Jolivet, J. Livage, *Struct. Bonding (Berlin)* **1992**, *77*, 155−206.
[22] D. C. Bradley, *Adv. Chem.* **1959**, *23*, 10−17.
[23] T. Moritz, J. Reiss, K. Diesner, D. Su, A. Chemseddine, *J. Phys. Chem. B* **1997**, *101*, 8052−8053.
[24] P. Pieranski, *Contemp. Phys.* **1983**, *24*, 25−73.
[25] A. Chemseddine, D. Tonti, M. Fieber-Erdmann, unpublished results.
[26] [26a] T. Sasaki, M. Watanabe, H. Hashizume, H. Yamada, H. Nakazawa, *J. Chem. Soc., Chem. Commun.* **1996**, 229−230. − [26b] T. Sasaki, M. Watanabe, H. Hashizume, H. Yamada, H. Nakazawa, *J. Am. Chem. Soc.* **1996**, *118*, 8325−8335. − [26c] T. Sasaki, M. Watanabe, *J. Phys. Chem. B* **1997**, *101*, 10159−10161.
[27] A. Firouzi, D. Kumar, L. M. Bull, T. Besier, P. Sieger, Q. Huo, S. A. Walker, J. A. Zasadzinski, C. Glinka, J. Nicol, D. Margolese, G. D. Stucky, B. F. Chmelka, *Science* **1995**, *267*, 1138−1143.
[28] A. Corma, *Chem. Rev.* **1997**, *97*, 2373−2419.

Received August 20, 1998
[I98288]